高功率涡旋拉曼光纤激光器

李阳　范晨晨　郝修路　马小雅　姚天甫　许将明　曾祥龙　周朴

High-power vortex Raman fiber laser

Li Yang, Fan Chenchen, Hao Xiulu, Ma Xiaoya, Yao Tianfu, Xu Jiangming, Zeng Xianglong, Zhou Pu

您可能感兴趣的其他文章

Articles you may be interested in

轨道角动量叠加态的产生及其检验

Generation of Orbital Angular Momentum superpositions and its test

红外与激光工程. 2018, 47(4): 417007　https://doi.org/10.3788/IRLA201847.0417007

光束轨道角动量谱的测量技术研究进展（特邀）

Advances on the measurement of orbital angular momentum spectra for laser beams (*Invited*)

红外与激光工程. 2021, 50(9): 20210145　https://doi.org/10.3788/IRLA20210145

涡旋光束的自适应光学波前校正技术研究进展（特邀）

Progress in adaptive optics wavefront correction technology of vortex beam (*Invited*)

红外与激光工程. 2021, 50(9): 20210428　https://doi.org/10.3788/IRLA20210428

利用超表面的涡旋光束产生进展（特邀）

Generation of optical vortex beams via metasurfaces (*Invited*)

红外与激光工程. 2021, 50(9): 20210283　https://doi.org/10.3788/IRLA20210283

直接输出的超短脉冲轨道角动量涡旋光产生技术研究进展（特邀）

Research progress on direct generation of ultrashort pulse OAM vortex beams (*Invited*)

红外与激光工程. 2020, 49(12): 20201061　https://doi.org/10.3788/IRLA20201061

轨道角动量模传输的圆环形光子晶体光纤

Circular photonic crystal fiber supporting orbital angular momentum modes transmission

红外与激光工程. 2019, 48(2): 222002　https://doi.org/10.3788/IRLA201948.0222002

高功率涡旋拉曼光纤激光器

李　阳[1]，范晨晨[1]，郝修路[1]，马小雅[1]，姚天甫[1,2,3*]，许将明[1]，曾祥龙[4]，周　朴[1]

(1. 国防科技大学 前沿交叉学科学院，湖南 长沙 410073；
2. 国防科技大学 南湖之光实验室，湖南 长沙 410073；
3. 高能激光技术湖南省重点实验室，湖南 长沙 410073；
4. 上海大学 特种光纤与光接入网重点实验室 特种光纤与
先进通信国际合作联合实验室，上海 200444)

摘　要： 近年来，携带轨道角动量的涡旋光束在激光加工、光学微粒操纵、超分辨成像、大容量光通信等领域应用广泛，目前已在稀土掺杂光纤激光器中得到了广泛研究。基于声致光纤光栅，实验搭建了全光纤结构拉曼光纤激光器，实现 LP_{01} 模与 LP_{11} 模的有效调控，并进一步通过偏振控制实现环形径向偏振光和拓扑荷数 $l=\pm1$ 的涡旋光束输出，最高输出功率~70 W，中心波长为 1 134 nm。文中提出的激光器有利于拓宽涡旋光束输出波段，在多维光通信、光场和物质相互作用等领域具备较大研究价值和应用潜力。

关键词： 拉曼光纤激光器；　涡旋光束；　声致光纤光栅；　轨道角动量

中图分类号： TN248　　　　**文献标志码：** A　　　　**DOI：** 10.3788/IRLA20230292

0　引　言

近年来，涡旋光束由于在光通信[1]、粒子加速[2]、微粒操控[3]、超分辨成像[4] 等领域具有重要研究价值和应用前景而备受关注。涡旋光束具有螺旋相位波前，同时每个光子携带轨道角动量 (Orbital angular momentum, OAM)，光强呈环形中空分布。目前，产生涡旋光场的方式主要分为两类：一类是是空间结构产生，例如通过超表面[5]、空间光调制器[6]、螺旋相位板[7]、q-波片[8] 等。自由空间中能产生的涡旋光场类型较多，例如通过空间光调制器，可以产生拓扑荷数 $l>50$ 的涡旋光[9]。但是空间结构不利于集成，且功率水平较为受限。另一类是光纤中产生，光纤具有波导模式稳定性，且光纤激光器具有结构紧凑，热管理方便，效率高等优点，利于实现高功率高稳定性涡旋光束输出。目前，全光纤激光器中实现涡旋光束主要利用少模光纤光栅[10]、长周期光纤光栅[11]、光子灯笼[12]、模式选择耦合器[13]、声致光纤光栅 (Acoustically-induced fiber grating, AIFG)[14-17] 等器件。其中，声致光纤光栅由于具有结构简单、波长调谐范围宽、响应速度快、插入损耗低等优点，在连续光激光器和超快锁模激光器中均得到广泛应用。例如，国防科技大学的吴函烁等人利用 AIFG 结合主振功率放大方案，实现了掺镱激光器中 LP_{11} 模的百瓦级放大，通过调控加载信号频率，实现模式切换，切换时间<1 ms[14]。进一步，结合偏振控制技术，上海大学利用 AIFG 实现了锁模激光器中的涡旋脉冲切换，并利用色散傅里叶变换首次观测了涡旋切换在锁模过程中的动力学演化过程[15]。西北工业大学基于 AIFG 在 1.5 μm 波段[16] 和绿光激光器[17] 中均实现了拓扑荷数 $l=\pm1$ 的轨道角动量光束输出。

随着大数据、云计算、物联网等技术的高速发展，拓展通信系统的信息容量刻不容缓。涡旋光束由于具备无限正交特性，可以大大提高通信系统容量。

2022 年, 中山大学通过特殊设计的七芯光纤, 每个纤芯支持 8 个 OAM 模式, 每个模式携带 10 个波长, 已经实验验证了其具备在 60 km 范围内传播 56 个 OAM 模式通道的能力[1]。而空分、模分、波分复用技术的结合, 亟需拓展涡旋光场的波长范围, 且特殊波段的涡旋光场还可以为研究光场与物质相互作用提供新的视角。Zhao 等人通过调节施加在手性长周期光纤光栅上的扭转力, 在 1.5 μm 波段实现 l = 1~3 的涡旋光束输出, 波长调谐范围约 20 nm[18]。上海理工大学采用涡旋波片和衍射光栅, 实现了 1015~1038 nm 波长的 l = ±1 涡旋脉冲输出[19]。近期, 北京邮电大学提出了一种等离激元超构表面辅助的波长可调谐 l = ±1 OAM 光束激光器, 波长调谐范围 1015~1075 nm[20], 输出功率约 5 mW, 激光器效率低于 10%。在光纤激光器中, 目前涡旋光束主要在掺镱、掺铒、掺铥等稀土离子发射波段产生, 而在其他波段增益较小, 拉曼激光技术为填补波长空白提供了新的思路。利用无源光纤中 13.2 THz 拉曼频移, 理论上只要有合适的泵浦源, 就可以实现任意波长的激光输出[21]。将声致光纤光栅应用于拉曼光纤激光器, 通过拉曼频移转换输出波长, 无需对模式转换器件参数进行重新设计和替换, 具有结构简单、无光子暗化、效率高等优点。

文中报道了基于声致光纤光栅, 在全光纤拉曼激光器中实现矢量偏振光束和拓扑荷数 l=±1 的涡旋光束输出, 输出激光中心波长为 1134.72 nm, 功率约 70 W。该实验不仅验证了声致光纤光栅超宽的模式转换特性, 有利于进一步丰富拓宽涡旋光束的应用, 也为全光纤高功率超宽波长可调谐涡旋光输出提供了新的思路。

1 实验装置和原理

搭建如图 1 所示的拉曼光纤振荡器。输出波长为 1080 nm 的掺镱光纤激光器作为泵浦源。反射率大于 99.5% 的高反射率光纤布拉格光栅 (High-reflective fiber Bragg grating, HR FBG) 和反射率为 19% 的低反射率光栅 (Low-reflective fiber Bragg grating, LR FBG) 构成振荡器的谐振腔。拉曼增益光纤为 200 m 长的渐变折射率 (Graded-index, GRIN) 光纤, 其纤芯直径为 20 μm, 数值孔径 NA 为 0.14, 折射率分布呈抛物线型。为了减少光纤熔接处的模场失配, HR FBG 与 LR

FBG 采用同种拉曼增益光纤刻写。拉曼光纤振荡器的输出模式为基模, 渐变折射率光纤的光束净化效应保证了输出基模的纯度[22]。AIFG 作为模式调控器件, 熔接在低反光栅之后, 可以将基模转换为 LP_{11} 模输出, 其所使用的光纤为少模阶跃折射率光纤, 纤芯直径 16 μm, 数值孔径 NA 为 0.11, 在 1080 nm 和 1130 nm 处支持 4 种 LP 模式, 分别为 LP_{01}、LP_{11}、LP_{21} 和 LP_{02} 模。为了控制输出模场偏振态, 在 AIFG 后连接三环式偏振控制器 (Polarization controller, PC), 其所用光纤与 AIFG 光纤相同。LP_{11} 模式由 4 个矢量模式简并而成, 通过旋转 PC, 可以调整 LP_{11} 模中矢量模式的耦合过程, 使所有的矢量模式都高效地耦合到某一特定矢量模或者产生特定相位差。为避免光纤端面反馈, 激光通过镀有增透膜的光纤端帽 (Endcap) 输出, 其在 1130 nm 波长的透过率大于 99.9%。

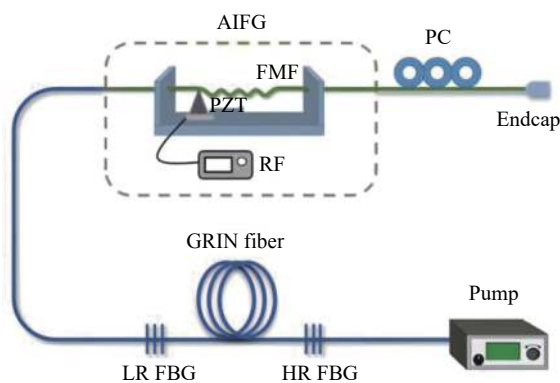

图 1 基于声致光纤光栅的涡旋拉曼光纤振荡器结构示意图

Fig.1 Schematic diagram of vortex Raman fiber oscillator based on acoustically-induced fiber grating (AIFG)

涡旋光束可以由 LP_{11} 模中的简并矢量模叠加产生, 产生涡旋光束可以基于对 LP_{11} 的偏振选择。AIFG 是产生 LP_{11} 模式的关键器件, 其基本结构如图 1 绿色虚线框内所示, 由压电陶瓷 (Piezoelectric transducer, PZT)、射频 (Radio frequency, RF) 信号源和少模光纤 (Few-mode fiber, FMF) 构成。在实验中, 射频信号源包含信号发生器和电压放大器两部分, 其中信号发生器先产生特定频率 (约数百 kHz) 的正弦信号, 再由电压放大器将此信号放大 50 倍。放大后的信号加载至压电陶瓷, 压电陶瓷将以与所施加信号相同的频率振动产生声波并传输至剥去涂覆层的少模光纤中。周期性的声致振动将在光纤中传播, 最终形成类似于长

周期光纤光栅的折射率调制机制，光栅周期为 $\Lambda=\sqrt{(\pi R C_{ext}/f)}$[23]，其中 R 是少模光纤的包层半径，$C_{ext}=5760$ m/s 为声波在石英光纤中的传播速度，f 为加载电信号的频率。根据模式耦合理论，LP_{01} 模和 LP_{11} 模在满足模式耦合条件 $\Lambda = L_B = \lambda/(n_{01}-n_{11})$[24] 时可以发生耦合。其中 λ 为传输激光波长，n_{01} 和 n_{11} 分别为 LP_{01} 模和 LP_{11} 模的有效折射率。为了测试 AIFG 加载信号频率与波长对应关系，基于弯曲损耗高阶模的原理，利用宽带光源测试 AIFG 的基模透射谱，如图 2(a) 所示。通过改变加载信号频率和电压，从 1050~1150 nm 波段透射谱可达到 12~16 dB，意味着从 LP_{01}~LP_{11} 模的转换具有较高的转换效率，其中在 1134 nm 处达到 16 dB (97%)，对应频率和电压

分别为 787 kHz 和 68.5 V。如图 2(b) 所示，射频信号频率与波长呈线性关系，其斜率约为 1.2 nm/kHz。

2 实验结果和分析

输出信号光功率随泵浦光功率的变化曲线图如图 3(a) 所示，其中黑色、红色曲线分别表示输出模式为 LP_{01} 模和 LP_{11} 模。当泵浦功率达到拉曼阈值后，信号光功率迅速增加，其中 LP_{01} 模最高输出功率为 70.8 W，斜率效率为 92.4%，LP_{11} 模最高输出功率为 69.6 W，斜率效率为 90.6%，此时总光光效率 83%。当泵浦功率高于 65 W 后，开始产生二阶拉曼光，其波长与激光器谐振波长不一致，导致斜率效率下降。曲线两侧展示了在不同功率水平时两种模式的光斑，分别
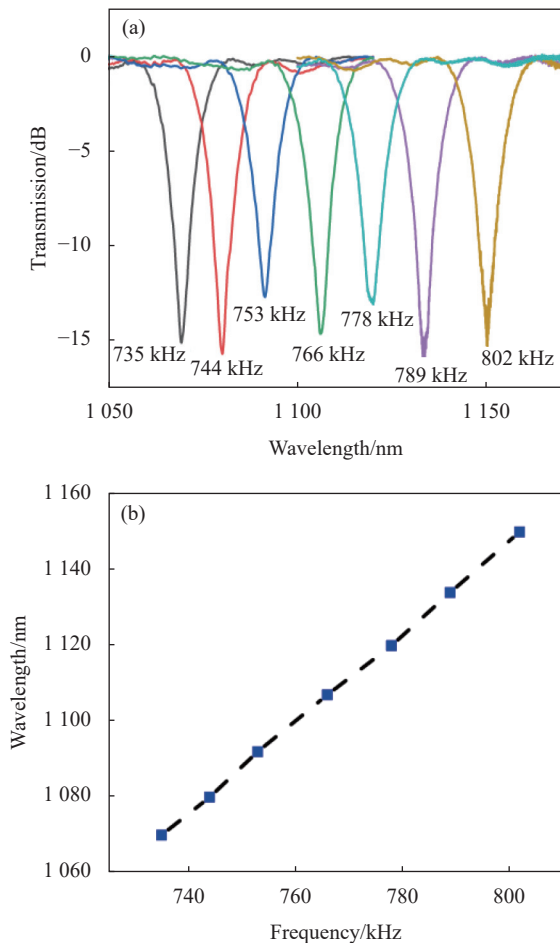

图 2 (a) 加载不同频率信号时 LP_{01} 模透射谱；(b) 特征频率与波长拟合曲线

Fig.2 (a) Transmission spectrum of LP_{01} mode at different loaded frequencies; (b) Fitted curve between the electrical frequency and wavelength
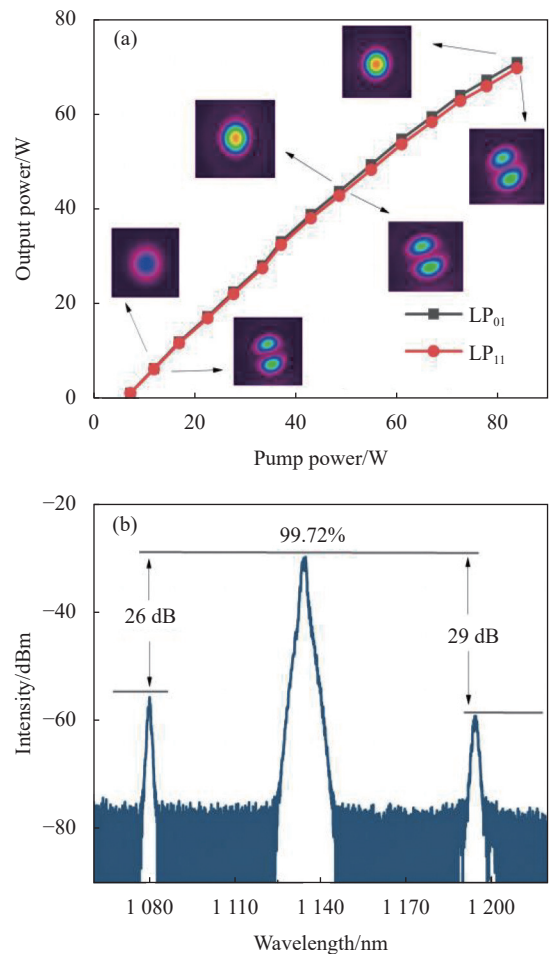
图 3 (a) 信号光功率随泵浦光功率变化和对应光斑；(b) 最高功率下的光谱

Fig.3 (a) Output signal power as a function of pump power and beam spots at corresponding power; (b) Spectrum at the maximum output power

为典型的 LP_{01} 模和 LP_{11} 模强度分布。输出 LP_{11} 模功率略低于 LP_{01} 模，是由于 AIFG 工作时引入额外损耗。由于 AIFG 在激光器输出端调控模式，两个模式输出光谱无明显差别。最高功率时输出光谱如图 3(b) 所示，输出信号光中心波长为 1 134.72 nm，中心波长为 1 194.16 nm 的二阶拉曼光限制了进一步功率提升。但在最高功率时，信号光仍高于二阶拉曼光 29 dB，高于泵浦光 26 dB，信号光光谱纯度达到 99.72%。

　　进一步，通过调整 PC 调节矢量模式耦合过程，可以使所有模式都高效地耦合到 TM_{01} 模，得到径向偏振光输出。如图 4(a) 所示，为原始光强分布，通过旋转线偏振片检测输出光束的模场分布，经过偏振片后的光斑如图 4(b1)~(b4) 所示，其中红色箭头表示偏振方向，随着偏振方向旋转，光斑的两瓣随之旋转并总是平行于偏振方向，可以确定产生了径向偏振 TM_{01} 模式。进一步，当偏振控制器使得光纤中的矢量模式产生 $\pi/2$ 相位差时，可以叠加产生涡旋光束，搭建迈克尔逊干涉仪，通过光斑自干涉法[25]，使涡旋光与具有一定横向位移的自身光斑干涉，可以检测到两个相反方向的"Y"形干涉条纹，如图 4(c) 和 4(d) 所示，其中插图为环形横向模场分布，在相同的干涉仪测量条件

下，得到两个对应"Y"形开口恰好相反的干涉图样，证明产生了拓扑荷数为 $l=\pm1$ 的 OAM 光束。

3　结　论

　　文中基于声致光纤光栅在拉曼光纤激光器中实现了径向偏振光和拓扑荷数 $l=\pm1$ 的涡旋光束输出，具有结构紧凑、波长调谐范围宽、响应速度快、插入损耗低等优点。输出中心波长 1 134.72 nm，光谱纯度 99.72%，功率~70 W，效率 83%。作为全光纤模式转换器件，声致光纤光栅超宽的波长调谐能力和高功率承受能力，有望使其成为填补涡旋光束光谱空白的关键器件，为特殊波段涡旋光束应用探索提供可靠的光源。通过更换泵浦源、增益光纤和级联拉曼频移，可以将波长覆盖范围进一步扩大，为大功率特殊波段涡旋光束提供可靠的种子源，并有望为大容量光通信系统提供光源。
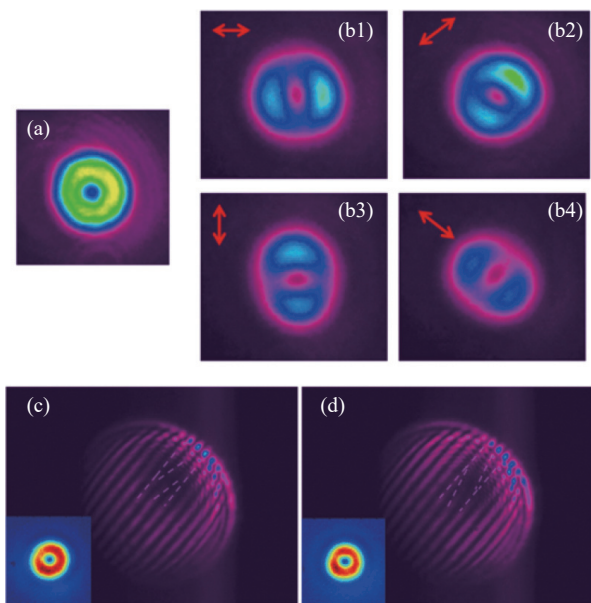

图 4 (a) 原始光强分布；(b1)~(b4) 经过线偏振片后的光强分布，其中红色箭头表示偏振方向；(c)、(d) 光斑自干涉条纹

Fig.4 (a) Original light intensity distribution; (b1)-(b4) Beam profiles after the linear polarizer, where the red arrows refer to the polarization direction; (c), (d) Self-interference patterns

参考文献：

[1] Zhang J, Lin Z, Liu J, et al. SDM transmission of orbital angular momentum mode channels over a multi-ring-core fibre [J]. *Nanophotonics*, 2021, 11(4): 873-884.

[2] Shi Y, Blackman D R, Zhu P, et al. Electron pulse train accelerated by a linearly polarized Laguerre–Gaussian laser beam [J]. *High Power Laser Science and Engineering*, 2022, 10: e45.

[3] Yang Y, Ren Y, Chen M, et al. Optical trapping with structured light: A review [J]. *Advanced Photonics*, 2021, 3(3): 034001.

[4] Willig K I, Keller J, Bossi M. STED microscopy resolves nanoparticle assemblies [J]. *New Journal of Physics*, 2006, 8(6): 106.

[5] Lv H, Bai Y, Ye Z, et al. Generation of optical vortex beams via metasurfaces(invited) [J]. *Infrared and Laser Engineering*, 2021, 50(9): 20210283. (in Chinese)

[6] Ma W, Lu H, Wang J, et al. Vortex beam generation based on spatial light modulator and deep learning [J]. *Acta Optica Sinica*, 2021, 41(11): 1107001. (in Chinese)

[7] Fridman M, Nixon M, Dubinskiy M, et al. Fiber amplification of radially and azimuthally polarized laser light [J]. *Physics*, 2010, 35(1): 1332-1334.

[8] Gregg P, Mirhosseini M, Rubano A, et al. Q-plates as higher order polarization controllers for orbital angular momentum modes of fiber [J]. *Optics Letters*, 2015, 40(8): 1729-1732.

[9] Ma X, Ye J, Zhang Y, et al. Vortex random fiber laser with

controllable orbital angular momentum mode [J]. *Photonics Research*, 2021, 9(2): 266-271.

[10] Sun B, Wang A, Xu L, et al. Low-threshold single-wavelength all-fiber laser generating cylindrical vector beams using a few-mode fiber Bragg grating [J]. *Optics Letters*, 2012, 37(4): 464-466.

[11] Zhao Y, Wang T, Mou C, et al. All-fiber vortex laser generated with few-mode long-period gratings [J]. *IEEE Photonics Technology Letters*, 2018, 30(8): 752-755.

[12] Lu Y, Liu W, Chen Z, et al. Spatial mode control based on photonic lanterns [J]. *Optics Express*, 2021, 29(25): 41788-41797.

[13] Wang T, Wang F, Shi F, et al. Generation of femtosecond optical vortex beams in all-fiber mode-locked fiber laser using mode selective coupler [J]. *Journal of Lightwave Technology*, 2017, 35(11): 2161-2166.

[14] Wu H, Xu J, Huang L, et al. High-power fiber laser with real-time mode switchability [J]. *Chinese Optics Letters*, 2022, 20(2): 021402.

[15] Lu J, Shi F, Meng L, et al. Real-time observation of vortex mode switching in a narrow-linewidth mode-locked fiber laser [J]. *Photonics Research*, 2020, 8(7): 1203-1212.

[16] Zhang W, Wei K, Huang L, et al. Optical vortex generation with wavelength tunability based on an acoustically-induced fiber grating [J]. *Optics Express*, 2016, 24(17): 19278-19285.

[17] Zhang W, Huang L, Wei K, et al. High-order optical vortex generation in a few-mode fiber via cascaded acoustically driven vector mode conversion [J]. *Optics Letters*, 2016, 41(21): 5082-5085.

[18] Zhao X, Liu Y, Liu Z, et al. Wavelength tunable OAM mode converters based on chiral long-period gratings [J]. *IEEE Photonics Technology Letters*, 2020, 32(24): 1519-1522.

[19] Hu H, Chen Z, Cao Qian, et al. Wavelength-tunable and OAM-switchable ultrafast fiber laser enabled by intracavity polarization control [J]. *IEEE Photonics Journal*, 2023, 15(1): 1-4.

[20] Gui L, Wang C, Ding F, et al. 60 nm span wavelength-tunable vortex fiber laser with intracavity plasmon metasurfaces [J]. *ACS Photonics*, 2023, 10(3): 623-631.

[21] Zhou P, Yao T, Fan C, et al. 50th anniversary of Raman fiber laser: History, progress and prospect (Invited) [J]. *Infrared and Laser Engineering*, 2022, 51(1): 20220015. (in Chinese)

[22] Terry N B, Alley T G, Russell T H. An explanation of SRS beam cleanup in graded-index fibers and the absence of SRS beam cleanup in step-index fibers [J]. *Optics Express*, 2007, 15(26): 17509-17519.

[23] Blake J N, Kim B Y, Engan H E, et al. Analysis of intermodal coupling in a two-mode fiber with periodic microbends [J]. *Optics Letters*, 1987, 12(4): 281-283.

[24] Vengsarkar A M, Pedrazzani J R, Judkins J B, et al. Long-period fiber-grating-based gain equalizers [J]. *Optics Letters*, 1996, 21(5): 336-338.

[25] Lan B, Liu C, Rui D, et al. The topological charge measurement of the vortex beam based on dislocation self-reference interferometry [J]. *Physica Scripta*, 2019, 94: 055502.

High-power vortex Raman fiber laser

Li Yang[1], Fan Chenchen[1], Hao Xiulu[1], Ma Xiaoya[1], Yao Tianfu[1,2,3*],

Xu Jiangming[1], Zeng Xianglong[4], Zhou Pu[1]

(1. College of Advanced Interdisciplinary Studies, National University of Defense Technology, Changsha 410073, China;

2. Nanhu Laser Laboratory, National University of Defense Technology, Changsha 410073, China;

3. Hunan Provincial Key Laboratory of High Energy Laser Technology, Changsha 410073, China;

4. Key Laboratory of Specialty Fiber Optics and Optical Access Networks, Joint International Research Laboratory of Specialty Fiber Optics and Advanced Communication, Shanghai University, Shanghai 200444, China)

Abstract:

Objective　In recent years, vortex beams carrying orbital angular momentum (OAM) have attracted much attention due to their important research value and application prospects in optical communication, particle acceleration, particle manipulation, super-resolution imaging, and other fields. At present, vortex optical field can be mainly divided into two types, one is generated by spatial devices, such as the spatial light modulator, and the

other is generated in fiber. Fiber lasers possess the advantages of compact structure, convenient thermal management, and high efficiency, which is conducive to realize the output of high-power and high-stability vortex beam. With the rapid development of big data, cloud computing, Internet of Things, and other technologies, it is urgent to expand the information capacity of communication systems. Vortex beams can greatly improve the capacity of communication systems because of their infinite orthogonality. At present, the output vortex beams of fiber lasers are mainly concentrated in the emission bands of rare earth ions such as ytterbium-doped, erbium-doped and thulium-doped, and the combination of space division, mode division and wavelength division multiplexing technology urgently needs to expand the wavelength range of the vortex beam. For this purpose, an all-fiberized vortex Raman fiber laser (RFL) is designed.

Methods   At present, many devices can realize vortex beam output in a fiber laser. Among them, the acoustically-induced fiber grating (AIFG) has the advantages of simple structure, wide wavelength tuning range, fast response speed and low insertion loss. Combined with the AIFG and RFL, when the output wavelength is converted by Raman frequency shift, there is no need to redesign and replace the mode conversion device. The RFL is built (Fig.1). The laser resonator is composed of a pair of fiber Bragg gratings and gain fiber. The AIFG is fused after the cavity. To control the polarization state of the output mode, a three-loop polarization controller (PC) is connected after AIFG. And the transmission spectrum of the LP_{01} mode is tested (Fig.2(a)), which indicates that there is a linear relationship between the frequency and the wavelength. Once the suitable electrical signal is loaded on the AIFG, the output mode is converted to LP_{11} mode, and the ring-shaped radially polarized light and vortex beam with topological charge $l=\pm1$ output can be realized by precise polarization control.

Results and Discussions   The variation curve of the output signal optical power with the pump optical power is shown (Fig.3(a)), where the black and red curves correspond to the output mode of LP_{01} mode and LP_{11} mode, respectively. The maximum output power of LP_{11} mode is 69.6 W, with a slope efficiency of 90.6% and total optical efficiency of 83%. The output spectrum at the highest power is shown (Fig.3(b)). The central wavelength of the output laser is 1 134.72 nm, and the second-order Raman light with a central wavelength of 1 194.16 nm restricts further power improvement. At the highest power, the spectral purity of signal light reaches 99.72%. By adjusting the PC, the radially polarized light output can be obtained. The mode field distribution of the output beam is detected by rotating the linear polarizer (Fig.4(b1)-(b4)), which verifies the radially polarized TM_{01} mode. Once there is a $\pi/2$ phase difference between the HE_{21}^{even} and HE_{21}^{odd} mode, the vortex beam can be realized through the superposition of the two modes, and the "Y-shaped" interference fringe can be detected through the self-interference (Fig.4(c)-(d)), which proves that the vortex beam with topological charge $l=\pm1$ is generated.

Conclusions   An all-fiberized Raman fiber laser with radially polarized light and vortex beam with topological charge $l=\pm1$ output is realized based on AIFG. It has the advantages of compact structure, wide wavelength tuning range, fast response speed and low insertion loss. The output central wavelength is 1 134.72 nm, with the spectral purity of 99.72%. The maximum output power is ~70 W, and the efficiency is 83%. As an all-fiberized mode conversion device, the AIFG is expected to be the key device to fill in the gaps in the spectrum of vortex beams due to its ultra-wide wavelength tuning ability and high power tolerable capacity, which could provide a reliable light source for the application and exploration of vortex beams in special waveband. By replacing the pump source and the gain fiber, the wavelength coverage can be extended further through cascaded Raman shift.

Key words: Raman fiber laser;   vortex beam;   acoustically-induced fiber grating;   orbital angular momentum